Available online at www.sciencedirect.com
ScienceDirect
Journal of Computational Physics 226 (2007) 156–179
JOURNAL OF COMPUTATIONAL PHYSICS
www.elsevier.com/locate/jcp

A stochastic Lagrangian approach for geometrical uncertainties in electrostatics

Nitin Agarwal, N.R. Aluru *

Department of Mechanical Science and Engineering, Beckman Institute for Advanced Science and Technology, University of Illinois at Urbana-Champaign, 405 N. Mathews Avenue, Urbana, IL 61801, United States

Received 18 September 2006; received in revised form 20 March 2007; accepted 29 March 2007
Available online 7 April 2007

Abstract

This work proposes a general framework to quantify uncertainty arising from geometrical variations in the electrostatic analysis. The uncertainty associated with geometry is modeled as a random field which is first expanded using either polynomial chaos or Karhunen–Loève expansion in terms of independent random variables. The random field is then treated as a random displacement applied to the conductors defined by the mean geometry, to derive the stochastic Lagrangian boundary integral equation. The surface charge density is modeled as a random field, and is discretized both in the random dimension and space using polynomial chaos and classical boundary element method, respectively. Various numerical examples are presented to study the effect of uncertain geometry on relevant parameters such as capacitance and net electrostatic force. The results obtained using the proposed method are verified using rigorous Monte Carlo simulations. It has been shown that the proposed method accurately predicts the statistics and probability density functions of various relevant parameters.

Keywords: Spectral stochastic boundary element method (SSBEM); Polynomial chaos; Lagrangian electrostatic analysis; Geometrical uncertainty

1. Introduction

An electrostatic analysis is required in applications such as – computational analysis of micro electromechanical systems (MEMS) [1–3] to compute the electrostatic force acting on the microstructures, modeling of interconnect circuits to extract the capacitance [4], etc. Over the years, various approaches have been used to compute the surface charge density accurately and efficiently. A boundary integral equation has been presented in [5] to treat the exterior electrostatics problem [6] in an efficient manner. A Lagrangian boundary integral equation has been derived in [7] to efficiently compute the surface charge density for the case of

* Corresponding author. Tel.: +1 217 333 1180; fax: +1 217 244 4333.
E-mail address: aluru@uiuc.edu (N.R. Aluru).
URL: http://www.uiuc.edu/~aluru (N.R. Aluru).

0021-9991/$ - see front matter
doi:10.1016/j.jcp.2007.03.026

deformable conductors. These methods assume that the geometry of the conductors in known in a deterministic sense. However, based on the manufacturing processes used, there is always some geometrical uncertainty associated with the conductors such as the dimensions or the gap between the electrodes, etc. Moreover, in applications where various physical fields interact in addition to the electrical field, uncertainties in the geometry of the conductors may occur indirectly due to uncertainty in parameters relevant to physical fields other than the electrical field. For example, for the computational analysis of MEMS, we need to model the interaction of mechanical, electrical and possibly fluidic energy domains [8]. Uncertainties associated with the mechanical or fluidic fields, such as the Young's modulus, etc., may result in an uncertain deformation and, hence, uncertain geometry of the conductors. In order to accurately compute the surface charge density and other output parameters such as capacitance and electrostatic force, etc., it is required to account for these geometrical variations in the numerical simulation. Specifically, the problem that we pose here is as follows – consider the two conductors as shown in Fig. 1, such that the geometry of one (or both) of the conductors is uncertain. The problem then is to quantify the uncertainty associated with the surface charge density resulting from the given variation in the geometry of the conductors.

The computational methods available to model uncertainties can be broadly classified into two major categories – methods based on a statistical approach and methods based on a non-statistical approach. The statistical approach includes methods such as classical Monte Carlo simulations [9,10] and various sampling schemes [11–13] such as stratified sampling, Latin hypercube sampling, etc. Since the accuracy of these methods depends on the sample size, simulations can become prohibitively expensive, especially for situations where it is expensive to solve the problem even in the deterministic case.

The most important non-statistical approach pioneered by Ghanem and Spanos [14] is *polynomial chaos*. Polynomial chaos is essentially a spectral expansion of the stochastic processes in terms of the orthogonal polynomials as given by Wiener's homogeneous chaos theory [15]. The homogeneous chaos expansion is based on *Hermite* polynomials and leads to fast converging algorithms when the underlying random variables are Gaussian. This idea was further generalized by Xiu and Karniadakis [16], to obtain exponentially converging algorithms even for non-Gaussian random variables, and has been applied to model uncertainty in various problems such as diffusion [17], fluid flow [18] and transient heat conduction [19].

The polynomial chaos expansion forms basis for the spectral stochastic finite-element method (SSFEM), where the uncertainty is treated as an additional dimension and the field variables are expanded along the random dimension using polynomial chaos expansion. SSFEM has been applied to a variety of problems [20–23], including those with uncertainty in their boundary conditions [24,25]. A stochastic Lagrangian approach based on SSFEM is presented in [26] for quantifying uncertainty propagation in finite deformation problems. Dasgupta et al. [27] explored the stochastic boundary element method (SBEM) to model the variation in geometry. A spectral stochastic boundary element method (SSBEM) has been presented in [28] to model geometrical uncertainties in elastostatic and elastodynamic problems. The uncertainty in boundary geometry is represented using Karhunen–Loève expansion, and the variation of the boundary matrices associated with the geometrical fluctuations is approximated by the Taylor expansion.

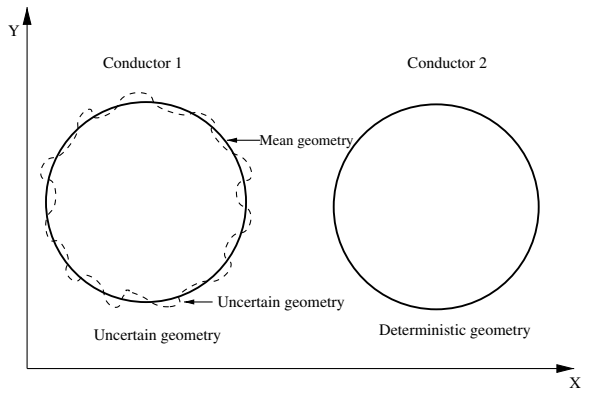

Fig. 1. A two-conductor system with uncertain geometry.

This work presents a general framework to quantify uncertainty associated with the surface charge density and various outputs of the electrostatic analysis such as capacitance and net electrostatic force, arising from uncertain geometry. The uncertainty associated with the geometry is modeled as a random field which is first expanded using either polynomial chaos or Karhunen–Loève expansion in terms of independent random variables. The random field is then treated as a random displacement applied to the conductors defined by the mean geometry, to derive the stochastic Lagrangian boundary integral equation in a manner analogous to the Lagrangian boundary integral equation for the case of deformable conductors [7]. The surface charge density is modeled as a random field, and is discretized both in random dimension and space using polynomial chaos and classical boundary element method, respectively. Various numerical examples are presented and the results obtained using the proposed method are verified using rigorous Monte Carlo simulations.

The paper is organized as follows: In Section 2, we first present two most widely used expansions – Karhunen–Loève (KL) expansion and Polynomial Chaos expansion, to represent random fields in terms of independent random variables. In Section 3, we present the Lagrangian boundary integral formulation for the electrostatics problem. In Section 4, we then develop the stochastic Lagrangian boundary integral equation and describe the discretization procedure both in the random dimension and space. In Section 5, we present some numerical examples in order to demonstrate the proposed method to handle geometrical uncertainties in the electrostatic analysis. We finally conclude the discussion in Section 6.

2. Spectral stochastic representation

Let D be a domain in $\mathbb{R}^d$, $d = 1, 2$ and $\mathbf{x} \in D$. Let $(\Theta, B, \mathscr{P})$ denote a probability space, where Θ is the set of elementary events, B is the σ-algebra of events and $\mathscr{P}$ is the probability measure. The symbol θ specifies an elementary event in Θ and is referred to as the random dimension. Then, all real valued functions $\xi(\theta)$ defined on Θ are known as random variables and functions $w(\mathbf{x}, \theta)$ defined on $D \times \Theta$ are known as random fields or processes. Uncertainties can be described using these stochastic quantities – uncertain parameters are modeled as random variables and uncertain spatial functions are represented as random fields.

From a numerical viewpoint, the random fields need to be discretized both in the random dimension θ and the spatial dimension $\mathbf{x}$. Thus, we seek a stochastic discretization that represents a random field in terms of finite number of independent random variables. Here, we present two spectral expansion methods – Karhunen–Loève expansion (KLE) and polynomial chaos expansion (PCE), which are most widely used for the discretization of random fields [14,29].

2.1. Karhunen–Loève (KL) expansion

Let $w(\mathbf{x}, \theta)$ denote a random field, which we seek to discretize, with a correlation function $C(\mathbf{x_1}, \mathbf{x_2})$, where $\mathbf{x_1}$ and $\mathbf{x_2}$ are the spatial coordinates. The KL expansion is based on the spectral expansion in terms of the eigenfunctions of the covariance kernel $C(\mathbf{x_1}, \mathbf{x_2})$ [30]. By definition, the covariance kernel is bounded, symmetric and positive definite. This fact simplifies the analysis as it guarantees that all the eigenfunctions are mutually orthogonal and form a complete set. The KL expansion can be written as

$$w(\mathbf{x}, \theta) = \bar{w}(\mathbf{x}) + \sum_{i=1}^{\infty} \sqrt{\lambda_i} \xi_i(\theta) f_i(\mathbf{x}), \tag{1}$$

where $\bar{w}(\mathbf{x})$ is the mean of the random field and $\{\xi_i(\theta)\}$ forms a set of uncorrelated random variables. Moreover, f_i and λ_i form the eigenvector–eigenvalue pair of the covariance kernel such that,

$$\int_D C(\mathbf{x_1}, \mathbf{x_2}) f_i(\mathbf{x_2}) \, \mathrm{d}\mathbf{x_2} = \lambda_i f_i(\mathbf{x_1}). \tag{2}$$

In practice the expansion in Eq. (1) is truncated after a finite number of terms M, which leads to a truncation error ϵ_M. As compared to other expansion methods, which use some orthonormal functions $\{f_i\}$, the KL expansion is optimal in the sense that the mean-square error $\int_D \epsilon_M^2 \, \mathrm{d}\mathbf{x}$ is minimized.

The applicability of the KL expansion depends on the ability to solve the integral equation (2). For certain choices of the covariance kernel and domain D, analytical solution exists for Eq. (2) as given in [14]. However, for general cases, we need to employ a numerical solution procedure, which is detailed in [14]. We must note that KL expansion requires the covariance function of the random field being expanded, which in general is not known *a priori*. Hence, KL expansion can only be used to represent the uncertain input random fields, for which the covariance structure is known. However, it cannot be implemented for a random field, which may be the unknown in a stochastic partial differential equation (SPDE), since its covariance function and therefore its eigenfunctions are not known. This problem can be avoided by using an alternative expansion, as described next.

2.2. Polynomial chaos expansion

The polynomial chaos expansion is essentially a spectral expansion of the random field in terms of the orthogonal polynomials in multi-dimensional random variables. The original polynomial chaos [15] employs *Hermite* polynomials in terms of the Gaussian random variables, and such an expansion converges to any L_2 function in the probability space in accordance with the Cameron–Martin theorem [31]. Let $\{\xi_i(\theta)\}_{i=1}^{\infty}$ be a set of orthonormal Gaussian random variables. Using this, the polynomial chaos expansion of a second-order random process or field $w(\mathbf{x},\theta)$ is given as

$$\begin{aligned} w(\mathbf{x},\theta) = a_0(\mathbf{x})\Gamma_0 + \sum_{i_1=1}^{\infty} a_{i_1}(\mathbf{x})\Gamma_1(\xi_{i_1}(\theta)) + \sum_{i_1=1}^{\infty}\sum_{i_2=1}^{\infty} a_{i_1 i_2}(\mathbf{x})\Gamma_2(\xi_{i_1}(\theta),\xi_{i_2}(\theta)) \\ + \sum_{i_1=1}^{\infty}\sum_{i_2=1}^{\infty}\sum_{i_3=1}^{\infty} a_{i_1 i_2 i_3}(\mathbf{x})\Gamma_3(\xi_{i_1}(\theta),\xi_{i_2}(\theta),\xi_{i_3}(\theta)) + \ldots, \end{aligned} \tag{3}$$

where $\Gamma_n(\xi_{i_1},\ldots,\xi_{i_n})$ denotes the polynomial chaos of order n in terms of the multi-dimensional Gaussian random variables $\boldsymbol{\xi} = (\xi_1,\ldots,\xi_n,\ldots)$. For convenience, Eq. (3) is often rewritten as

$$w(\mathbf{x},\theta) = \sum_{i=0}^{\infty} \hat{a}_i(\mathbf{x})\Psi_i(\boldsymbol{\xi}(\theta)), \tag{4}$$

where there is a one-to-one correspondance between the functions $\Gamma[\cdot]$ and $\Psi[\cdot]$ and also between the coefficients $a_{i_1 i_2 \ldots}$ and $\hat{a}_i$. For the case of one-dimensional Hermite polynomial chaos, $\boldsymbol{\xi} = \xi_1 = \xi$ and $\{\Psi_i\}$ are simply the one-dimensional Hermite polynomials given as

$$\Psi_0(\xi) = 1, \quad \Psi_1(\xi) = \xi, \quad \Psi_2(\xi) = \xi^2 - 1, \quad \Psi_3(\xi) = \xi^3 - 3\xi, \quad \Psi_4(\xi) = \xi^4 - 6\xi^2 + 3, \ldots \tag{5}$$

The functions $\{\Psi_i\}$ form an orthogonal basis in the probability space, with the orthogonality relation

$$\langle \Psi_i, \Psi_j \rangle = \delta_{ij}\langle \Psi_i^2 \rangle, \tag{6}$$

where δ_{ij} is the Kronecker delta and $\langle \cdot,\cdot \rangle$ denotes the ensemble average which is the inner product given as

$$\langle \Psi_i, \Psi_j \rangle = \int_{\Theta} \Psi_i(\boldsymbol{\xi})\Psi_j(\boldsymbol{\xi})\,\mathrm{d}\mathscr{P}. \tag{7}$$

For the case of Hermite polynomial chaos, $\mathrm{d}\mathscr{P}$ is the Gaussian probability measure $\mathrm{e}^{-\frac{1}{2}\boldsymbol{\xi}^{\mathrm{T}}\boldsymbol{\xi}}\,\mathrm{d}\boldsymbol{\xi}$. We note that the summation in Eq. (3) is infinite and also each polynomial chaos $\Gamma[\cdot]$ is a function of the infinite set $\{\xi_i(\theta)\}_{i=1}^{\infty}$, and is therefore an infinite dimensional Hermite polynomial. However, in practice it is logical to use a finite-dimensional set $\{\xi_i(\theta)\}_{i=1}^{n}$, which yields an n-dimensional polynomial chaos expansion. Also, we truncate the summation in Eq. (3) up to some finite order p. Thus, the expansion in Eq. (4) can now be written as

$$w(\mathbf{x},\theta) = \sum_{i=0}^{N} \hat{a}_i(\mathbf{x})\Psi_i(\boldsymbol{\xi}(\theta)). \tag{8}$$

The total number of terms included in the polynomial chaos expansion $(N+1)$, depends both on the dimensionality n and the highest order p of the multi-dimensional polynomials used, and is given as

$$N+1=\frac{(n+p)!}{n!p!}. \tag{9}$$

Although in theory, the Hermite chaos converges to any L_2 functionals in the random space, it achieves optimal exponential convergence rates only for Gaussian or near Gaussian random fields. A more general framework, known as the *generalized polynomial chaos* was developed in [16], where the polynomials are chosen from the hypergeometric polynomials of the Askey scheme and the underlying random variables are not restricted to Gaussian random variables. The type of the random variables is selected based on the random inputs, and their weighting function in turn decides the type of orthogonal polynomials used as basis in the chaos expansion. For example, Jacobi polynomials are chosen for Beta random variables and Legendre polynomials are chosen as basis for uniform random variables. The optimal exponential convergence rate was also demonstrated for the choice of these bases. In this work, for all the examples, we assume the stochastic inputs to be defined using Gaussian random variables, and hence Hermite polynomials are used as basis in the chaos expansion.

3. Deterministic Lagrangian electrostatics

In this section, we first present the deterministic Lagrangian boundary integral formulation for the electrostatic analysis of deformable conductors. We consider a two conductor system as shown in Fig. 2. We denote the initial or undeformed configuration of the two conductors by Ω_1 and Ω_2 with surface or boundaries as $\mathrm{d}\Omega_1$ and $\mathrm{d}\Omega_2$, respectively. The deformed configuration is denoted by ω_1 and ω_2, respectively, with boundaries $\mathrm{d}\omega_1$ and $\mathrm{d}\omega_2$, respectively. The domain exterior to the two conductors is denoted by $\bar{\omega}$. The electrical potential ϕ is prescribed on the surface of the two conductors. The objective of the deterministic problem is to find the surface charge density in the undeformed configuration.

3.1. Lagrangian boundary integral equations

The exterior electrostatics problem on $\bar{\omega}$ can be solved efficiently by employing a boundary integral formulation [5] as follows:

$$\phi(p)=\int_{\mathrm{d}\omega} G(p,q)\sigma(q)\,\mathrm{d}\gamma_q + C, \tag{10}$$

$$C_{\mathrm{T}}=\int_{\mathrm{d}\omega}\sigma(q)\,\mathrm{d}\gamma_q, \tag{11}$$

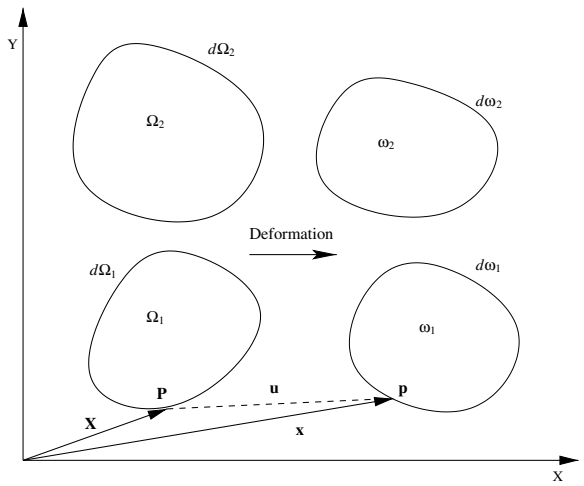

Fig. 2. A two conductor system under deformation.

where σ is the unknown surface charge density, p is the source point, q is the field point, G is the Green's function, $d\gamma_q$ represents an infinitesimal line segment at a specified field point q and $d\omega = d\omega_1 \cup d\omega_2$. In two dimensions, $G(p,q) = -\frac{\ln|p-q|}{2\pi\epsilon}$, where $|p-q|$ is the distance between the source and the field point and ϵ is the permittivity of free space. C_T represents the total charge of the system, which is set to be zero and C is an unknown which needs to be computed. Since the integrals in this formulation refer to the deformed configuration, we need to constantly update the geometry whenever the conductors deform.

A Lagrangian approach has been derived in [7] which allows to solve for surface charge density in the deformed configuration, by solving the electrostatics equations on the undeformed configuration. Since the stochastic Lagrangian formulation presented later is derived in an analogous manner, we include some details on the derivation of deterministic formulation as given in [7]. As shown in Fig. 2, we consider a point P on the boundary $d\Omega_1$ of conductor 1 with the position vector $\mathbf{X}$ and an infinitesimal boundary segment with length $d\Gamma$ originating from P. As conductor 1 deforms, point P undergoes a displacement $\mathbf{u}$ and moves to p with the position vector $\mathbf{x}$ and the length of the infinitesimal boundary segment changes from $d\Gamma$ to $d\gamma$. The position of a point $\mathbf{x}$ and the length of an infinitesimal line segment $d\gamma$ in the deformed configuration can be mapped to the corresponding quantities in the undeformed configuration, denoted by $\mathbf{X}$ and $d\Gamma$, respectively as:

$$\mathbf{x} = \mathbf{X} + \mathbf{u}, \tag{12}$$

$$d\gamma = (\mathbf{T}\cdot\mathbf{C}\mathbf{T})^{1/2} d\Gamma, \tag{13}$$

where $\mathbf{T}$ is the unit tangent vector to $d\Omega_1$ at point P and $\mathbf{C} = \mathbf{F}^{\mathrm{T}}\mathbf{F}$ is the Green deformation tensor. $\mathbf{F}$ is the deformation gradient tensor given by

$$F_{ij} = \frac{\partial x_i}{\partial X_j} = \delta_{ij} + \frac{\partial u_i}{\partial X_j} \quad i,j = 1,2 \quad \text{for 2D}. \tag{14}$$

Using Eqs. (12) and (13) in Eqs. (10) and (11), the *Lagrangian boundary integral equations* are given by:

$$\phi(P) = \int_{d\Omega} G(p(P), q(Q))\sigma(q(Q))[\mathbf{T}(Q)\cdot\mathbf{C}(Q)\mathbf{T}(Q)]^{\frac{1}{2}} d\Gamma_Q + C, \tag{15}$$

$$C_T = \int_{d\Omega} \sigma(q(Q))[\mathbf{T}(Q)\cdot\mathbf{C}(Q)\mathbf{T}(Q)]^{\frac{1}{2}} d\Gamma_Q, \tag{16}$$

where P and Q refer to the positions of source and field points, respectively, in the undeformed configuration $d\Omega = d\Omega_1 \cup d\Omega_2$, $\mathbf{C}(Q) = \mathbf{F}^{\mathrm{T}}(Q)\mathbf{F}(Q)$, $\mathbf{F}(Q)$ being the deformation gradient tensor and $\mathbf{T}(Q)$ being the tangential vector at the field point Q in the undeformed configuration. We note that the integrals in Eqs. (15) and (16) are defined on the boundaries in undeformed configuration $d\Omega$, and all the quantities inside the integrals are also appropriately mapped to the initial configuration.

3.2. Spatial discretization – boundary element method

The Lagrangian boundary integral equations (15) and (16) can be solved numerically using the classical boundary element method (BEM) [32]. In the classical BEM, the surface of the conductors is discretized into segments or panels and the unknown surface charge density is approximated by using interpolation functions. The surface charge density $\sigma(\mathbf{x}(\mathbf{X}))$ at a point $\mathbf{x}$ in the deformed configuration is given as

$$\sigma(\mathbf{x}(\mathbf{X})) = \sum_{k=1}^{K} \sigma_k N_k(\mathbf{X}), \tag{17}$$

where K is the total number of panels, σ_k is the value of surface charge density at point k and $N_k(\mathbf{X})$ is the interpolation function of point k evaluated at $\mathbf{X}$. In the collocation method, the centroid of each panel is treated as a collocation point and the interpolation functions are taken to be piecewise constant, such that the interpolation function corresponding to each panel is unity for that panel and zero elsewhere. This also implies that the surface charge density is constant over each panel. Using this in Eqs. (15) and (16) we get,

$$\phi(P) = \sum_{k=1}^{K} \int_{d\Omega_k} -\frac{1}{2\pi\epsilon} \ln|P + \mathbf{u}_P - Q_k - \mathbf{u}_{Q_k}| \sigma_k [\mathbf{T}(Q_k) \cdot \mathbf{C}(Q_k)\mathbf{T}(Q_k)]^{\frac{1}{2}} d\Gamma_{Q_k} + C, \tag{18}$$

$$C_T = \sum_{k=1}^{K} \int_{d\Omega_k} \sigma_k [\mathbf{T}(Q_k) \cdot \mathbf{C}(Q_k)\mathbf{T}(Q_k)]^{\frac{1}{2}} d\Gamma_{Q_k}, \tag{19}$$

where $d\Omega_k$ is the length of the kth panel in the undeformed configuration, Q_k is the field point on the kth panel, $\mathbf{u}_P$ and $\mathbf{u}_{Q_k}$ are the displacements at the source point P and the field point Q_k, respectively and σ_k is the constant surface charge density for the kth panel. This leads to the matrix-form as follows:

$$[M]\{\Sigma\} = \{\Phi\}, \tag{20}$$

where M is a $(K+1) \times (K+1)$ matrix and Σ and Φ are $(K+1) \times 1$ unknown and right-hand side vectors, respectively. The entries of matrix M are given as

$$M(i,j) = \int_{d\Omega_j} -\frac{1}{2\pi\epsilon} \ln|P_i + \mathbf{u}_{P_i} - Q_j - \mathbf{u}_{Q_j}| [\mathbf{T}(Q_j) \cdot \mathbf{C}(Q_j)\mathbf{T}(Q_j)]^{\frac{1}{2}} d\Gamma_{Q_j} \quad i,j = 1,\ldots,K$$

$$M(K+1,j) = \int_{d\Omega_j} [\mathbf{T}(Q_j) \cdot \mathbf{C}(Q_j)\mathbf{T}(Q_j)]^{\frac{1}{2}} d\Gamma_{Q_j} \quad j = 1,\ldots,K$$

$$M(i,K+1) = 1 \quad i = 1,\ldots,K$$

$$M(K+1,K+1) = 0.$$

Also the vectors Σ and Φ are defined as

$$\Sigma = \begin{Bmatrix} \sigma_1 \\ \sigma_2 \\ \cdot \\ \cdot \\ \sigma_K \\ C \end{Bmatrix} \quad \Phi = \begin{Bmatrix} \phi(P_1) \\ \phi(P_2) \\ \cdot \\ \cdot \\ \phi(P_K) \\ C_T \end{Bmatrix}. \tag{21}$$

The surface charge density $\sigma(\mathbf{x})$ can be obtained by solving the linear system given by Eq. (20).

3.3. Computation of outputs

In certain situations the objective of the electrostatic analysis may not be restricted to the computation of surface charge density, but we may also require to compute certain outputs which depend on the surface charge density. For example, in the modeling of interconnect circuits or micro-electromechanical (MEMS) sensors, we might need to compute the self and mutual capacitances of the conductors, for which we need to compute the total charge on all the conductors. The total charge in the undeformed configuration on conductor 1 can be computed as

$$Q = \int_{d\Omega_1} \sigma(\mathbf{x}) [\mathbf{T} \cdot \mathbf{CT}]^{\frac{1}{2}} d\Gamma. \tag{22}$$

The analysis of MEMS actuators requires the computation of electrostatic pressure, which is then used to compute the deformation of microstructures, using a mechanical analysis. The electrostatic pressure at $\mathbf{x}$ in the deformed configuration $\mathbf{h}(\mathbf{x})$, is given as [33]

$$\mathbf{h}(\mathbf{x}) = \frac{\sigma^2(\mathbf{x})}{2\epsilon} \mathbf{n}(\mathbf{x}), \tag{23}$$

where $\mathbf{n}(\mathbf{x})$ is the unit outward normal at $\mathbf{x}$ in the deformed configuration. The electrostatic pressure at $\mathbf{X}$ in the undeformed configuration $\mathbf{H}(\mathbf{X})$, can be written as [7]

$$\mathbf{H}(\mathbf{X}) = \frac{\sigma^2(\mathbf{x}(\mathbf{X}))}{2\epsilon} J[\mathbf{F}(\mathbf{X})]^{-T}\mathbf{N}(\mathbf{X}), \tag{24}$$

where J is the determinant of $\mathbf{F}(\mathbf{X})$ and $\mathbf{N}(\mathbf{X})$ is the outward unit normal at $\mathbf{X}$ in the undeformed configuration.

4. Stochastic Lagrangian electrostatics

Having described the Lagrangian boundary integral formulation for the case of deformable conductors, we now proceed to develop the stochastic formulation to handle the geometrical uncertainties. Unlike the previous case, the geometry of the conductors is not known in a deterministic sense and hence the surface integrals in the boundary integral equations (10) and (11) cannot be computed. However, this difficulty of having to compute the surface integrals in the uncertain configuration can be circumvented by using the Lagrangian boundary integral formulation. The idea is to express the geometry of the conductors as a sum of its mean, known as the mean configuration, and a zero-mean random field, which represents the uncertainty associated with this mean configuration. The zero-mean random field is then treated as a random displacement applied to the conductors defined by the mean configuration, to develop a stochastic Lagrangian formulation analogous to the case with deterministic deformation. In the stochastic formulation, the mean geometry is analogous to the initial or undeformed configuration and the uncertain geometry is analogous to the deformed configuration. The objective of this approach is to compute the surface charge density in the uncertain configuration using the mean configuration.

4.1. Stochastic Lagrangian boundary integral equations

The displacement $\mathbf{u}(\mathbf{X},\theta)$ is modeled as a random field which depends both on space and the random dimension θ. Using the techniques described in Section 2, we write a spectral expansion for the random displacement $\mathbf{u}(\mathbf{X},\theta)$ as

$$\mathbf{u}(\mathbf{X},\theta) = \sum_{m=0}^{M} \mathbf{u}_m(\mathbf{X})\Psi_m(\theta), \tag{25}$$

where $M+1$ is the total number of terms considered in the KL expansion or polynomial chaos expansion, to represent the random displacement field. In this work, since we do not have any physical deformation for the conductors, $\mathbf{u}(\mathbf{X},\theta)$ is considered as a zero-mean random field. However, in situations when in addition to the geometrical uncertainties, the conductors also undergo some actual deformation (deterministic or random), the displacement $\mathbf{u}(\mathbf{X},\theta)$ would have a non-zero mean. Such situations can also be handled using this approach in a straightforward manner.

In a manner similar to the deterministic case, we can define various physical quantities in the uncertain (deformed) configuration in terms of the quantities in the mean (undeformed or initial) configuration. To begin with, the position of a point on the uncertain boundary can be written as

$$\mathbf{x} = \mathbf{X} + \mathbf{u}(\mathbf{X},\theta). \tag{26}$$

Using Eq. (26) the stochastic Green's function in two dimensions $G(p,q,\theta)$ can be written as

$$G(p,q,\theta) = G(p(P),q(Q),\theta) = -\frac{1}{2\pi\epsilon}\ln|P - Q + \mathbf{u}_P(\theta) - \mathbf{u}_Q(\theta)|, \tag{27}$$

where P and Q are the source and field points in the mean configuration, p and q are the source and field points in the uncertain configuration, and $\mathbf{u}_P(\theta)$ and $\mathbf{u}_Q(\theta)$ are the random displacements associated with P and Q, respectively. We can further compute the stochastic deformation gradient $\mathbf{F}(\mathbf{X},\theta)$ as

$$F_{ij} = \frac{\partial x_i}{\partial X_j} = \delta_{ij} + \sum_{m=0}^{M} \frac{\partial u_{m,i}}{\partial X_j}\Psi_m(\theta) \quad i,j = 1,2 \quad \text{for 2D}, \tag{28}$$

where $u_{m,i}$ denotes the ith component of the mth displacement mode vector $\mathbf{u}_m$.

As in Eq. (13), we can express the length of an infinitesimal line element $d\gamma_q$ at a specified field point q in the uncertain configuration in terms of the length of the corresponding line element $d\Gamma_Q$ at the field point Q in the mean configuration as:

$$d\gamma_q = d\Gamma_Q[\mathbf{T}(Q)\cdot\mathbf{C}(Q,\theta)\mathbf{T}(Q)]^{\frac{1}{2}}, \tag{29}$$

where $\mathbf{C}(\mathbf{X},\theta) = \mathbf{F}^{\mathrm{T}}\mathbf{F}$ is the stochastic Green deformation tensor and $\mathbf{T}(Q)$ is the tangent at the field point Q.

Using Eqs. (27) and (29) we can write the *Stochastic Lagrangian boundary integral equations* for electrostatics, analogous to Eqs. (15) and (16) for the deterministic case as follows:

$$\phi(P) = \int_{d\Omega} G(p(P),q(Q),\theta)\sigma(q(Q),\theta)[\mathbf{T}(Q)\cdot\mathbf{C}(Q,\theta)\mathbf{T}(Q)]^{\frac{1}{2}}d\Gamma_Q + C(\theta), \tag{30}$$

$$C_{\mathrm{T}} = \int_{d\Omega} \sigma(q(Q),\theta)[\mathbf{T}(Q)\cdot\mathbf{C}(Q,\theta)\mathbf{T}(Q)]^{\frac{1}{2}}d\Gamma_Q, \tag{31}$$

where $d\Omega = d\Omega_1 \cup d\Omega_2$ represents the mean or undeformed configuration, $C(\theta)$ is an unknown random variable and C_{T} is the total charge, which is set to be zero. We note that all the integrals in Eqs. (30) and (31) are defined over the mean configuration $d\Omega$ and all the quantities inside the integrals are appropriately defined in terms of the quantities in the mean configuration. By defining $\gamma(Q,\theta) = [\mathbf{T}(Q)\cdot\mathbf{C}(Q,\theta)\mathbf{T}(Q)]^{\frac{1}{2}}$, Eqs. (30) and (31) can be written as

$$\phi(P) = \int_{d\Omega} G(p(P),q(Q),\theta)\sigma(q(Q),\theta)\gamma(Q,\theta)d\Gamma_Q + C(\theta) \tag{32}$$

$$C_{\mathrm{T}} = \int_{d\Omega} \sigma(q(Q),\theta)\gamma(Q,\theta)d\Gamma_Q. \tag{33}$$

4.2. Stochastic discretization – polynomial chaos

Due to the random nature of the problem, in addition to the spatial discretization we also need to consider the discretization with respect to the random dimension θ. We write the polynomial chaos expansion for the unknown surface charge density $\sigma(\mathbf{x},\theta)$, and the random variable $C(\theta)$ as follows:

$$\sigma(\mathbf{x},\theta) = \sum_{n=0}^{N}\sigma_n(\mathbf{x})\Psi_n(\xi(\theta)), \quad C(\theta) = \sum_{n=0}^{N} C_n\Psi_n(\xi(\theta)), \tag{34}$$

where $(N+1)$ is the total number of terms considered in the truncated polynomial chaos expansion. We note that the uncertainty associated with the surface charge density is included in the polynomial basis $\Psi(\xi(\theta))$ and hence the spectral modes $\sigma_n(\mathbf{x})$ and $C_n, n = 0,\ldots,N$ are deterministic. Now using the expansion given in Eq. (34) in Eqs. (32) and (33) and replacing $\Psi_n(\xi(\theta))$ by Ψ_n for clarity, we get,

$$\phi(P) = \int_{d\Omega} \mathcal{G}(P,Q,\theta)\left(\sum_{n=0}^{N}\sigma_n(q(Q))\Psi_n\right)d\Gamma_Q + \sum_{n=0}^{N} C_n\Psi_n, \tag{35}$$

$$C_{\mathrm{T}} = \int_{d\Omega} \gamma(Q,\theta)\left(\sum_{n=0}^{N}\sigma_n(q(Q))\Psi_n\right)d\Gamma_Q, \tag{36}$$

where $\mathcal{G}(P,Q,\theta) = G(p(P),q(Q),\theta)\gamma(Q,\theta)$. In order to compute the integrals in the random dimension efficiently, we express $\mathcal{G}(P,Q,\theta)$ and $\gamma(Q,\theta)$ in terms of the orthogonal polynomials $\{\Psi_l\}$ as explained later in Appendix A,

$$\mathcal{G}(P,Q,\theta) = \sum_{l=0}^{N}\mathcal{G}_l(P,Q)\Psi_l(\theta) \quad \gamma(Q,\theta) = \sum_{l=0}^{N}\gamma_l(Q)\Psi_l(\theta). \tag{37}$$

In order to ensure that the error is orthogonal to the space spanned by the finite dimensional basis functions $\{\Psi_m,\ m = 0,\ldots,N\}$, we employ Galerkin projection of the above equations onto each Ψ_m, which yields,

$$\phi(P)\langle\Psi_m\rangle = \int_{d\Omega} \sum_{n=0}^{N}\sum_{l=0}^{N} \mathscr{G}_l(P,Q)\sigma_n(q(Q))\langle\Psi_l\Psi_n\Psi_m\rangle d\Gamma_Q + C_m\langle\Psi_m^2\rangle, \quad m = 0,\ldots,N \tag{38}$$

$$C_T\langle\Psi_m\rangle = \int_{d\Omega} \sum_{n=0}^{N}\sum_{l=0}^{N} \gamma_l(Q)\sigma_n(q(Q))\langle\Psi_l\Psi_n\Psi_m\rangle d\Gamma_Q, \quad m = 0,\ldots,N \tag{39}$$

using the orthogonality relation $\langle\Psi_m,\Psi_n\rangle = \delta_{mn}\langle\Psi_m^2\rangle$, where $\langle\cdot\rangle = \langle\cdot,1\rangle$ represents the ensemble average. The above set of equations represent $2(N+1)$ coupled integral equations that need to be solved for $2(N+1)$ unknowns, $\sigma_n(\mathbf{x})$, C_n, $n = 0,\ldots,N$. We note that these equations are deterministic as the unknowns $\{\sigma_n(\mathbf{x})\}$ depend only on $\mathbf{x}$ and $\{C_n\}$ are constants.

4.3. Spatial discretization – BEM

At this point, we introduce the spatial discretization using BEM, as described earlier for the deterministic case and assume that each of $\sigma_n(\mathbf{x})$ is constant over each panel, such that

$$\sigma_n(\mathbf{x}(\mathbf{X})) = \sum_{k=1}^{K} \sigma_n^k N_k(\mathbf{X}), \quad n = 0,\ldots,N, \tag{40}$$

where $N_k(\mathbf{X}), k = 1,\ldots,K$ are the piecewise constant shape functions used for the collocation method and K is the total number of panels. To simplify the expressions we define

$$e_{mn}(P,Q) = \sum_{l=0}^{N} \mathscr{G}_l(P,Q)\langle\Psi_l\Psi_m\Psi_n\rangle, \quad m,n \in [0,N] \tag{41}$$

$$d_{mn}(Q) = \sum_{l=0}^{N} \gamma_l(Q)\langle\Psi_l\Psi_m\Psi_n,\rangle, \quad m,n \in [0,N], \tag{42}$$

where the integrals $\langle\Psi_l\Psi_m\Psi_n\rangle$ can be precomputed. Using the above notational simplifications and substituting the spatial discretization given in Eq. (40) in Eqs. (38) and (39) we get,

$$\phi(P)\langle\Psi_m\rangle = \sum_{n=0}^{N}\sum_{k=1}^{K} \int_{d\Omega_k} e_{mn}(P,Q_k)\sigma_n^k d\Gamma_k + C_m\langle\Psi_m^2\rangle, \quad m \in [0,N] \tag{43}$$

$$C_T\langle\Psi_m\rangle = \sum_{n=0}^{N}\sum_{k=1}^{K} \int_{d\Omega_k} d_{mn}(Q_k)\sigma_n^k d\Gamma_k, \quad m \in [0,N]. \tag{44}$$

This leads to a matrix system

$$\begin{bmatrix} [M]_{0,0} & \cdots & [M]_{0,N} \\ \vdots & [M]_{m,n} & \vdots \\ [M]_{N,0} & \cdots & [M]_{N,N} \end{bmatrix}_{Ns\times Ns} \begin{Bmatrix} \{\Sigma_1\}_{K\times 1} \\ \vdots \\ \{\Sigma_m\}_{K\times 1} \\ \vdots \\ \{\Sigma_N\}_{K\times 1} \end{Bmatrix}_{Ns\times 1} = \begin{Bmatrix} \{\Phi_1\}_{K\times 1} \\ \vdots \\ \{\Phi_m\}_{K\times 1} \\ \vdots \\ \{\Phi_N\}_{K\times 1} \end{Bmatrix}_{Ns\times 1}, \tag{45}$$

where $Ns = (K+1)(N+1)$, and the entries of $[M]_{m,n}, \{m,n = 0,\ldots,N\}$ are given as

$$M(i,j) = \int_{d\Omega_j} e_{mn}(P_i,Q_j)d\Gamma_k, \quad i,j = 1,\ldots,K \tag{46}$$

$$M(K+1,j) = \int_{d\Omega_j} d_{mn}(Q_j)d\Gamma_k, \quad j = 1,\ldots,K \tag{47}$$

$$M(i,K+1) = \langle\Psi_m,\Psi_n\rangle, \quad i = 1,\ldots,K \tag{48}$$

$$M(K+1,K+1) = 0. \tag{49}$$

The vectors Σ_m and Φ_m, $m = 0, \ldots, N$ are defined as

$$\Sigma_m = \begin{Bmatrix} \sigma_m^1 \\ \sigma_m^2 \\ \cdot \\ \cdot \\ \cdot \\ \sigma_m^K \\ C_m \end{Bmatrix} \quad \Phi_m = \langle \Psi_m \rangle \begin{Bmatrix} \phi(P_1) \\ \phi(P_2) \\ \cdot \\ \cdot \\ \cdot \\ \phi(P_K) \\ C_T \end{Bmatrix}. \tag{50}$$

The matrix system given in Eq. (45) can be solved to obtain the spectral modes $\sigma_n(\mathbf{x}), n \in [0, N]$.

4.4. Computation of relevant quantities

Having solved for the spectral modes $\{\sigma_n\}$, the surface charge density is obtained using Eq. (34):

$$\sigma(\mathbf{x}, \theta) = \sum_{n=0}^{N} \sigma_n(\mathbf{x}) \Psi_n(\xi(\theta)).$$

A random field $w(\mathbf{x}, \theta)$ is often characterized by its statistics defined as expectation $\mathbb{E}[\cdot]$:

$$\mathbb{E}[g(w)] = \int_{\Theta} g(w)\, \mathrm{d}\mathscr{P}, \tag{51}$$

where g is some suitable function. Noting that $\langle \Psi_0 \rangle = 1$ and $\langle \Psi_n \rangle = 0, \forall n > 0$, the mean of the surface charge density $\bar{\sigma}(\mathbf{x})$ is given as

$$\bar{\sigma}(\mathbf{x}) = \mathbb{E}[\sigma(\mathbf{x}, \theta)] = \sigma_0(\mathbf{x}). \tag{52}$$

The standard deviation of the surface charge density $v(\mathbf{x})$ can be obtained as

$$v^2(\mathbf{x}) = \mathbb{E}[(\sigma(\mathbf{x}, \theta) - \bar{\sigma}(\mathbf{x}))^2] = \sum_{n=1}^{N} \sigma_n^2(\mathbf{x}) \langle \Psi_n^2 \rangle, \tag{53}$$

using the orthogonality relation $\langle \Psi_m, \Psi_n \rangle = \delta_{mn} \langle \Psi_m^2 \rangle$.

As pointed out in the deterministic case, in addition to the surface charge density we may also need to compute the outputs such as, capacitance and force. In a similar fashion as Eq. (22), the total charge in the mean configuration on conductor 1 can be computed as

$$Q(\theta) = \int_{\mathrm{d}\Omega_1} \sigma(\mathbf{x}, \theta) [\mathbf{T} \cdot \mathbf{CT}]^{\frac{1}{2}} \mathrm{d}\Gamma = \sum_{n=0}^{N} Q_n(\theta) \Psi_n(\xi(\theta)), \tag{54}$$

where $Q_n(\theta) = \int_{\mathrm{d}\Omega_1} \sigma_n(\mathbf{x}) [\mathbf{T} \cdot \mathbf{CT}]^{\frac{1}{2}} \mathrm{d}\Gamma$. Also, using Eq. (24) the electrostatic pressure in the mean configuration $\mathbf{H}(\mathbf{x}, \theta)$, is given as

$$\mathbf{H}(\mathbf{X}, \theta) = \frac{\sigma^2(\mathbf{x}(\mathbf{X}), \theta)}{2\epsilon} J [\mathbf{F}(\mathbf{X}, \theta)]^{-\mathrm{T}} \mathbf{N}(\mathbf{X}), \tag{55}$$

where J is the determinant of $\mathbf{F}$ and $\mathbf{N}(\mathbf{X})$ is the unit outward normal at $\mathbf{X}$ in the mean configuration.

5. Examples

In this section, we present a few examples where we apply the approach developed in the previous section to model geometrical uncertainties in the electrostatic analysis. In the first set of examples, we consider the effect of variation in geometrical parameters during the modeling of interconnect circuits. As the smallest feature size in circuits drops to submicron levels, interconnect characteristics are becoming increasingly more impor-

tant. It has been shown that the interconnect parameters determine critical signal delays in circuits. Hence, in order to ensure the desired circuit performance, it becomes necessary to accurately model the effect of variations in these interconnect parameters during the design process. The effect of interconnect parameter variation on circuit performance using statistical methods such as Monte Carlo method, has been studied in [34,35]. Specifically, we consider two cases – single and double lines over a ground plane, and study the effect of variations in geometrical parameters on the capacitance.

In the second set of examples we consider the effect of geometrical uncertainties during the design of electrostatically actuated micro-electromechanical systems (MEMS). MEMS devices have been used in widespread applications such as micro-switches, micro-accelerometers, etc. These devices consist of microstructures that undergo deformation upon the application of an electrostatic actuation force. The electrostatic force is usually computed using numerical simulations, assuming that the geometry of the conductors in known in a deterministic sense. However, depending on the manufacturing processes used, there is always some uncertainty associated with geometrical features such as the dimension of the electrodes or the gap between the electrodes. In order to predict the effect of these variations and design reliable MEMS devices, it is required to accurately model these uncertainties during the design process. We specifically consider two cases – a transverse comb drive and a cantilever beam over a ground plane and study the effect of geometrical uncertainties on the capacitance and the net electrostatic force.

For all the examples considered in this work, we assume that the stochastic geometrical parameters are defined using Gaussian random variables. Since the actual distribution suitable to model uncertain geometrical features for micro-structures is not known, the Gaussian distribution is selected as it has been traditionally used to model uncertain parameters in practical applications. Theoretically, the unboundedness of the support of Gaussian random variables may lead to some problems in the implementation, as the geometrical features are certainly bounded. However, in practice we obtain meaningful results since for the expected level of uncertainty, the probability of these variables being unbounded is negligible.

5.1. Single line over a ground plane

Consider a rectangular wire with width $W = 1$ μm and thickness $T = 0.2$ μm, placed at a distance H from the ground plane as shown in Fig. 3a. We study the effect of variation in the gap H, on the capacitance between the wire and the ground plane. The gap is modeled as a random variable and is written as

$$H(\theta) = \overline{H}(1 + v_H \xi(\theta)), \tag{56}$$

where $\overline{H} = 0.2$ μm is the mean or average gap, ξ is a Gaussian random variable with unit variance and v_H is the percentage variation in H. It can be easily seen that the wire placed at a distance $\overline{H}$ from the ground plane represents the mean configuration of the two conductors and $v_H \overline{H} \xi$ represents variation in the gap. This variation in the gap is implemented by applying a random translational displacement to the wire in the vertical direction, given as $\mathbf{u}(\mathbf{x}, \theta) = [0, v_H \overline{H} \xi]^{\mathrm{T}}$. This displacement can also be identified as the spectral expansion given in Eq. (25) with only the second term as non-zero, which represents a zero-mean Gaussian random variable.

The surface charge density profile for the mean configuration, obtained using deterministic boundary integral formulation Eq. (20) is shown in Fig. 4a. The potentials for the wire and the ground plane are set to be unity and zero, respectively.

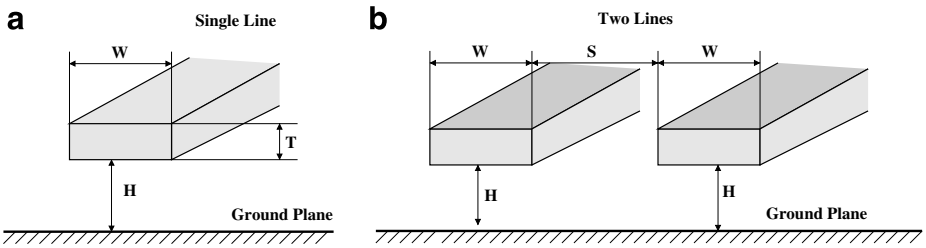

Fig. 3. Cross section of interconnect structures. (a) Single line over a ground plane. (b) Double line over a ground plane.

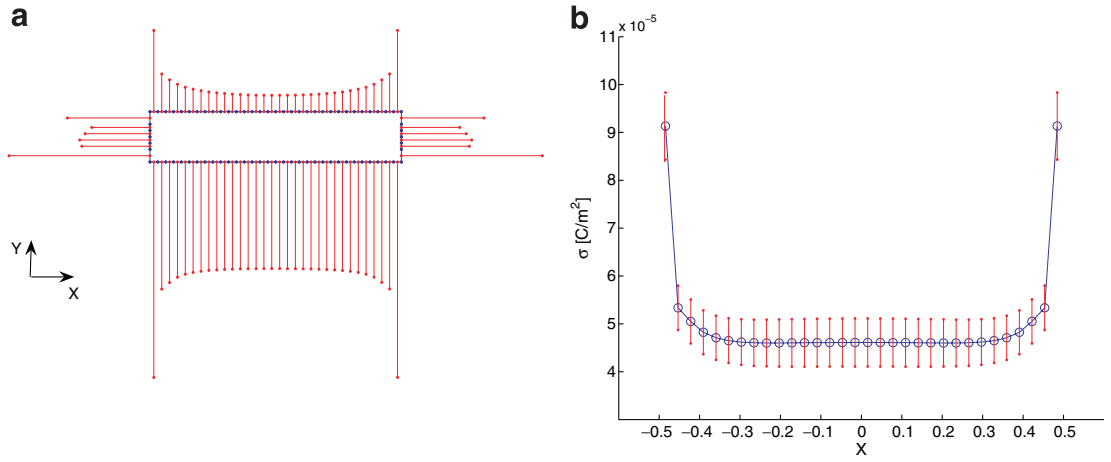

Fig. 4. Surface charge density on the single line. (a) Surface charge density profile in the mean configuration using BEM. (b) Mean $\bar{\sigma}(\mathbf{x})$ with error bars $\pm v(\mathbf{x})$ on the bottom surface for $v_H = 0.1, \phi_{\text{line}} = 1$ V, $\phi_{\text{ground}} = 0$ V.

We first set $v_H = 0.1$, which corresponds to a 10% variation in the gap and use a polynomial chaos expansion of order $p = 3$ in Eq. (34). The matrix system, given in Eq. (45), resulting from the stochastic Lagrangian formulation is then solved and the mean and standard deviation for the surface charge density are computed using Eqs. (52) and (53), respectively. The mean surface charge density $\bar{\sigma}(\mathbf{x})$, for the bottom surface of the wire is plotted along with the error bars $\pm v(\mathbf{x})$ in Fig. 4b.

We now study the effect of variation in H on the capacitance between the wire and the ground plane. In the deterministic case, the capacitance C_1 can be computed as

$$C_1 = \frac{Q}{V}, \tag{57}$$

where Q is the total charge on the wire, which can be computed using Eq. (22) and V is the applied potential on the wire. An empirical formula for the capacitance (per unit length) between a single line and the ground plane has been derived in [36] and is given as

$$\frac{C_1}{\epsilon} = 1.15\left(\frac{W}{H}\right) + 2.80\left(\frac{T}{H}\right)^{0.222}. \tag{58}$$

The relative error of this formula is shown to be within 6% for $0.3 < W/H < 30$ and $0.3 < T/H < 30$. In this formula, the first term can be considered as contribution from the lower surface of the line and the second term represents the side wall contribution. The capacitance in the mean configuration, obtained using the deterministic BEM formulation and Eq. (58) is shown in Fig. 5 for various values of H.

As shown in Fig. 5, there is a reasonable agreement between the capacitance values computed using the boundary integral formulation and the empirical formula over a range of H values. Hence, in addition to the Monte Carlo (MC) simulations, we also use Eq. (58) to verify the results obtained using the stochastic Lagrangian formulation. In the stochastic case, the capacitance $C_1(\xi(\theta))$ can be computed using Eq. (57) as for the deterministic case, but the random total charge on the wire is now computed using Eq. (54).

In Fig. 6 we plot the probability density function (PDF) of the capacitance using Monte Carlo (MC) simulations, polynomial chaos (PC) of several orders and the empirical formula Eq. (58), for $v_H = 0.1$ and 0.2, which corresponds to a variation of 10% and 20% in H, respectively. For MC simulations we use 30000 realizations of H (generated according to the Gaussian distribution), and corresponding to each realization the deterministic problem is solved and we obtain the capacitance values $\{C_1\}$. In order to get the PDFs using PC and the empirical formula, we generate realizations of ξ in accordance with the Gaussian distribution and obtain the values $\{C_1(\xi)\}$. For all the methods, a histogram of these $\{C_1\}$ values is then generated based on 50 equally spaced bins and the probability density is obtained by normalizing the frequency corresponding

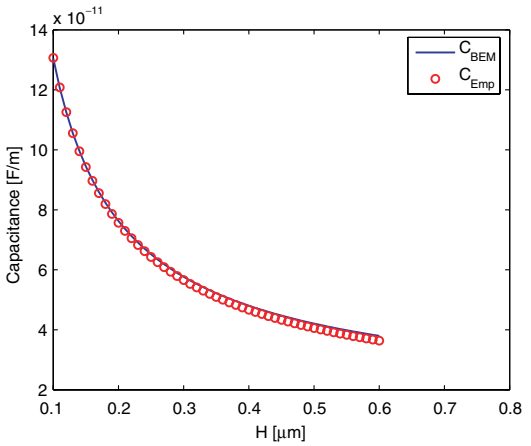

Fig. 5. Capacitance between the single line and ground plane obtained using BEM and empirical formula given in Eq. (58), $W = 1$ μm, $T = 0.2$ μm.

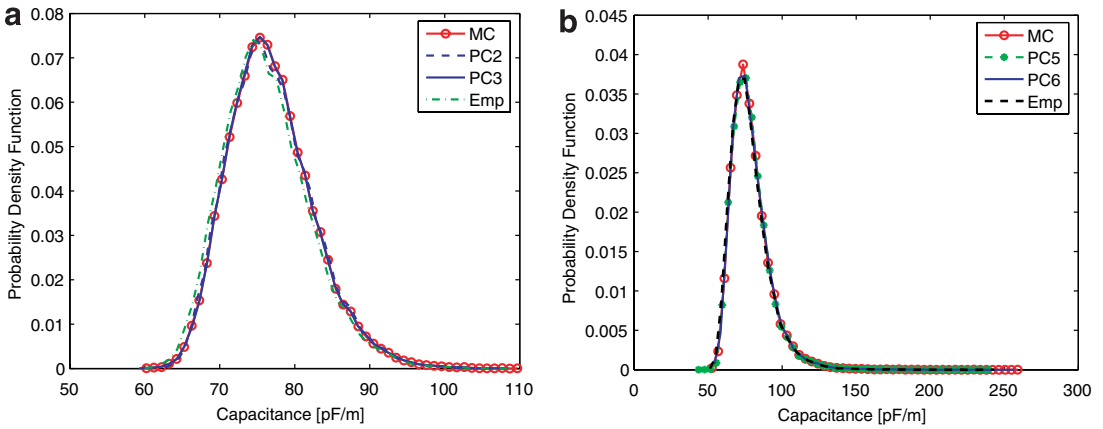

Fig. 6. Probability density function of capacitance between the single line and the ground plane for variation in gap H. (a) $v_H = 0.1$, 10% variation. (b) $v_H = 0.2$, 20% variation.

to each bin with the bin size and the total number of realizations. The PDFs are finally generated by plotting these probability density values along the centers of the bins.

As can be seen from Fig. 6a, for a 10% variation in H, there is a good agreement amongst the PDFs obtained using MC simulation, polynomial chaos of order $p = 3$ and the empirical formula. We also notice that the PDF obtained using PC expansion converges to the MC result, as we increase the expansion order p from 2 to 3. Similarly, as can be seen from Fig. 6b, for a 20% variation in H, the PDFs obtained using the three methods are again in good agreement. The convergence of the polynomial chaos expansion to the MC result, again improves with increasing order. We also notice that the order of the PC expansion required to obtain accurate results increases to 6 for the 20% variation case, as compared to 3 for the 10% variation case. The mean and standard deviation for the capacitance as obtained from different methods are shown in Tables 1 and 2, for the case of 10% and 20% variation, respectively.

Table 1
Mean and standard deviation for capacitance [$v_H = 0.1$]

	MC	PC2	PC3	Emp
Mean [pF/m]	76.8919	76.8918	76.8920	76.2580
Std [pF/m]	5.7482	5.7423	5.7481	5.8329

Table 2
Mean and standard deviation for capacitance, $[v_H = 0.2]$

	MC	PC4	PC5	PC6	Emp
Mean [pF/m]	78.8386	78.8396	78.8423	78.8427	78.1703
Std [pF/m]	13.5264	13.5201	13.5573	13.5614	13.5523

5.2. Double line over a ground plane

We now consider two identical lines separated by a distance S and placed over a ground plane at a distance H as shown in Fig. 3b, and study the effect of variation in these two parameters on the total capacitance of either line. Both the lines have rectangular cross-sections with width $W = 1$ μm and thickness $T = 0.2$ μm. The gap between the lines and ground plane H, and the separation between the lines S are modeled as random variables and are written as

$$H(\theta) = \overline{H}(1 + v_H\xi_1) \quad S(\theta) = \overline{S}(1 + v_S\xi_2), \tag{59}$$

where $\overline{H} = 0.2$ μm is the average gap and $\overline{S} = 0.15$ μm is the average separation distance between the lines, v_H and v_S represent the percentage variation in gap and separation, respectively. ξ_1 and ξ_2 are independent Gaussian random variables with unit variances. The mean configuration is represented by two wires separated by $\overline{S}$ and placed at a distance $\overline{H}$ from the ground plane. The variation in H and S is implemented by applying a random translational displacement $\mathbf{u}_L = [v_S\overline{S}\xi_2, v_H\overline{H}\xi_1]^{\mathrm{T}}$ to the wire on left, and $\mathbf{u}_R = [0, v_H\overline{H}\xi_1]^{\mathrm{T}}$ to the wire on right.

We set $v_H = 0.1$ and $v_S = 0.1$, which corresponds to a 10% variation in both H and S. For the stochastic Lagrangian formulation, we use two dimensional polynomial chaos expansions Eq. (34) which consist of 6 and 10 terms for order $p = 2$ and 3, respectively. As for the single line case, an empirical expression for the total capacitance of either line per unit length C_2, has been derived in [36] and is given as

$$\frac{C_2}{\epsilon_0} = \frac{C_1}{\epsilon_0} + \left[0.03\left(\frac{W}{H}\right) + 0.83\left(\frac{T}{H}\right) - 0.07\left(\frac{T}{H}\right)^{0.222}\right]\left(\frac{S}{H}\right)^{-1.34}, \tag{60}$$

where C_1 is given by Eq. (58). The relative error of this formula is shown to be within 10% for $0.3 < W/H < 10$, $0.3 < T/H < 10$ and $0.5 < S/H < 10$.

As shown in Fig. 7, there is a reasonable agreement between the capacitance values obtained using the deterministic BEM and the empirical formula given in Eq. (60) over a range of H and S. Hence, in addition to the MC simulations, we also use the empirical formula to verify the results obtained using stochastic for-

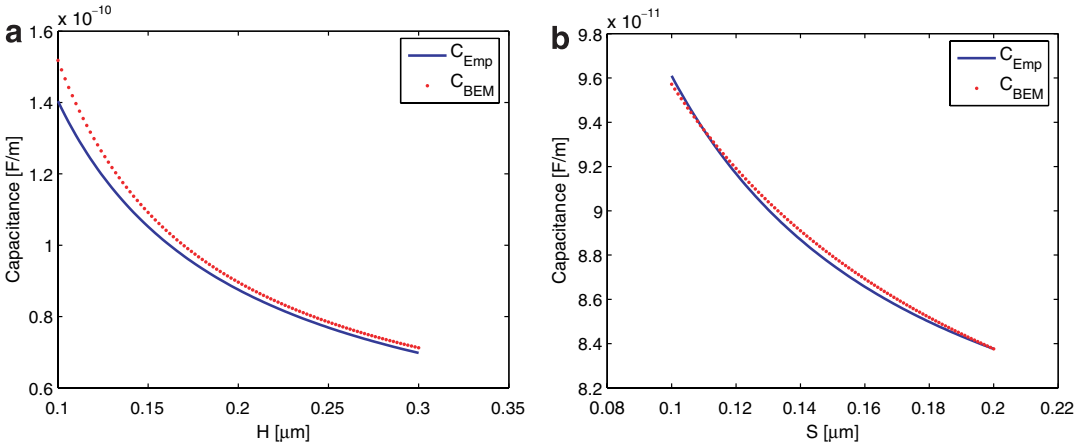

Fig. 7. Total capacitance of one wire computed using BEM and the empirical formula Eq. (60). (a) Variation of gap H, $S = 0.15$ μm. (b) Variation of separation S, $H = 0.2$ μm.

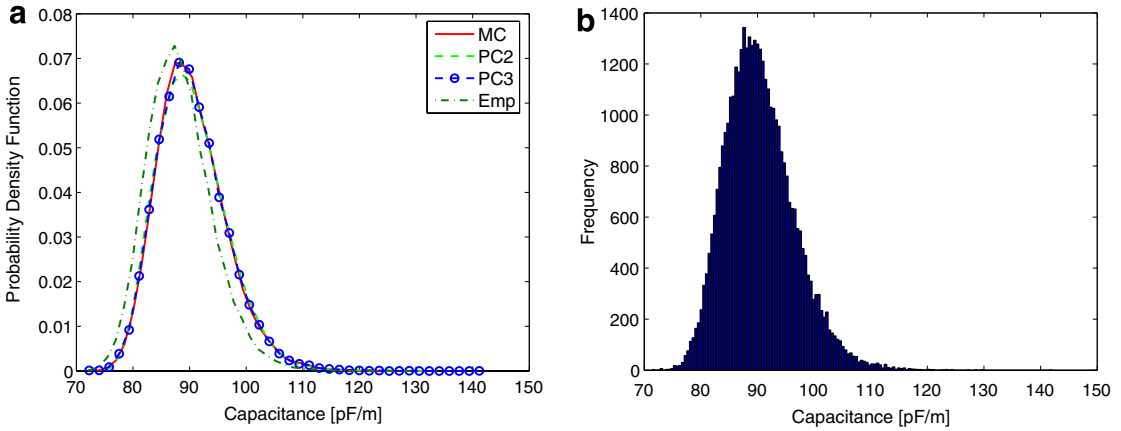

Fig. 8. Probability density functions for variation in gap between the lines and ground plane H, and separation between the lines S, $[v_H = 0.1, v_S = 0.1]$. (a) Probability density function of capacitance. (b) Histogram of capacitance using polynomial chaos expansion of order $p = 3$.

Table 3
Mean and standard deviation for capacitance $[v_H = 0.1, v_S = 0.1]$

	MC	PC2	PC3	Emp
Mean [pF/m]	90.4041	90.4011	90.4022	88.2696
Std [pF/m]	6.1416	6.1402	6.1532	5.7765

mulation. For the MC simulations, we use 40,000 samples each for ξ_1 and ξ_2 generated according to the Gaussian distribution, such that ξ_1 and ξ_2 are independent. We must note that it is possible to perform the MC simulations in a more efficient manner using various sampling schemes such as Latin–Hypercube sampling [13,11], etc. However, since we use MC simulations for verification purpose only, such sampling schemes have not been emphasized here.

In Fig. 8a, we plot the probability density functions for the total capacitance obtained using MC simulations, empirical formula and polynomial chaos expansion of several orders. The results obtained using polynomial chaos converge to the MC results as the order of expansion p is increased. A histogram plot for the capacitance obtained using polynomial chaos (order $p = 3$) is shown in Fig. 8b. The mean and standard deviation values for capacitance obtained using various methods are tabulated in Table 3.

5.3. Comb drive

Comb drives form an important class of MEMS devices and have been used in widespread applications such as micro-accelerometers, hard disk actuators and position controllers. Consider the transverse comb drive [37] as shown in Fig. 9. The system consists of a center movable stage supported on folded springs and an array of interdigitated teeth. An electrostatic force is generated when a potential difference is applied between the fixed teeth and the movable teeth attached to the center stage, which provides a vertical movement. Depending on the manufacturing process, there is always some uncertainty associated with the geometrical features such as the thickness of the movable fingers or fixed teeth, overlap length between the two set of teeth, etc. The effect of various geometrical features on the design of a comb drive has been studied in [38] using Monte Carlo method incorporated in the ANSYS probabilistic design system (ANSYS/PDS).

In this example, we consider one pair of teeth as shown in Fig. 9 to separately study the effect of variation in the thickness T and the length L of the movable teeth, on the capacitance and the net electrostatic force. In the mean configuration, the thickness is $\overline{T} = 4\ \mu m$ and the length is $\overline{L} = 60\ \mu m$. The smaller and larger gaps between the two electrodes are 2 μm and 5 μm, respectively. An electrical potential V is applied to the movable

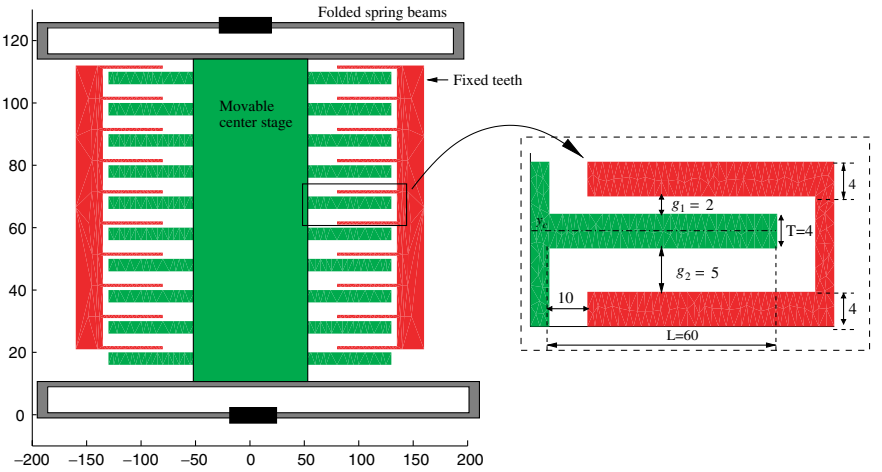

Fig. 9. Transverse comb drive (All dimensions are in μm).

tooth, while the fixed tooth is grounded. The surface charge density profile for the two teeth in the mean configuration, obtained using a deterministic analysis are shown in Fig. 10. First, we study the effect of variation in the thickness T of the movable finger, which is represented as

$$T(\theta) = \overline{T}(1 + v_T\xi), \tag{61}$$

where ξ is a Gaussian random variable with unit variance and v_T is the percentage variation in T. For this study, the length L is assumed to be fixed as the mean value $\overline{L} = 60$ μm. The variation in the thickness $v_T\overline{T}\xi$, is implemented by applying a random displacement which stretches the movable finger in a symmetric fashion about the horizontal center plane. The displacement is given as $\mathbf{u}(\mathbf{x}, \theta) = [0, v_T(y - y_c)\xi]^{\mathrm{T}}$, where y_c is the location of horizontal center plane passing through the movable finger. Using this displacement in the stochastic Lagrangian formulation, the random surface charge density is obtained.

Once the random surface charge density is computed, the capacitance between the two teeth can be computed as described earlier. For this case, in addition to the capacitance between the two teeth, we are also interested in computing the net electrostatic force acting on the movable finger. The net electrostatic force in the mean configuration can be obtained by first computing the random electrostatic pressure using Eq. (55) and then integrating it over the mean surface. For this study, we set $v_T = 0.1$, which corresponds to a variation of 0.4 μm in the thickness. In Fig. 11, we plot the probability density functions for the capacitance, and the horizontal and vertical components of the force for $V = 1$ V, using PC expansion of several orders and the MC simulations. For MC simulations 30,000 realizations have been used. The polynomial chaos results are not only in agreement with the Monte Carlo simulations, but the convergence also improves with increasing the order of the PC expansion used. In Fig. 11d, we plot the variation of the mean of the vertical force $\mathbb{E}[F_y]$ with applied voltage together with the corresponding error bars $\pm v_{F_y}$, where v_{F_y} represents the standard deviation in the vertical force. The mean and standard deviation in capacitance and force are tabulated in Table 4.

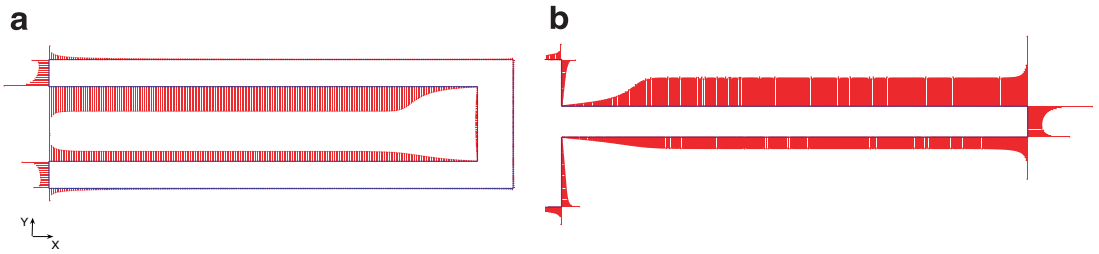

Fig. 10. Surface charge density profile on one pair of teeth for the transverse comb drive in the mean configuration, $V = 1$ V. (a) Fixed tooth. (b) Movable tooth.

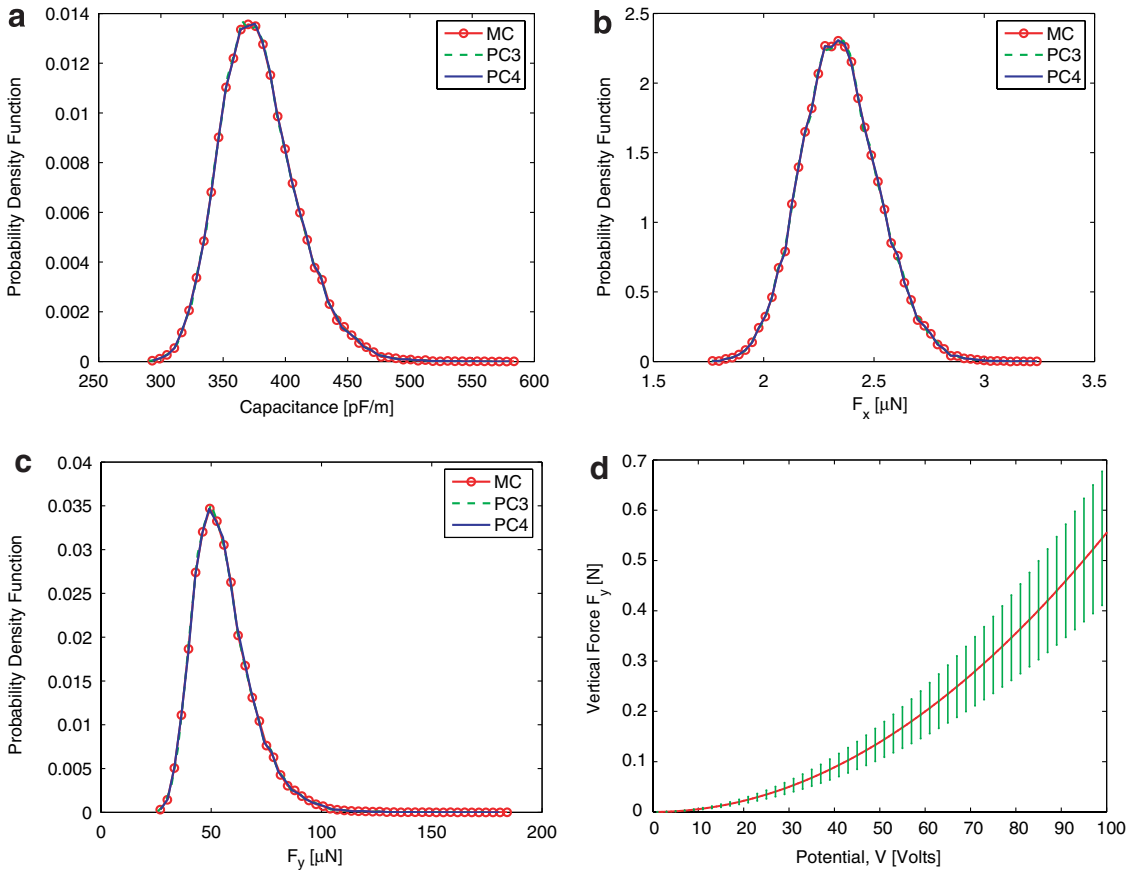

Fig. 11. Effect of 10% variation in the thickness of the movable finger in the transverse comb drive on capacitance and net electrostatic force. (a) Probability density function of capacitance. (b) Probability density function of horizontal force F_x. (c) Probability density function of vertical force F_y. (d) Variation of mean and corresponding error bars of the vertical force with applied voltage V.

Table 4
Mean and standard deviation of capacitance and force for 10% variation in T

		MC	PC3	PC4
Capacitance [pF/m]	Mean $\times 10^{-2}$	3.7854	3.7854	3.7854
	Std $\times 10^{-1}$	3.0946	3.0948	3.0949
Horizontal Force F_x [μN]	Mean $\times 10^{0}$	2.3461	2.3462	2.3462
	Std $\times 10^{1}$	1.7610	1.7612	1.7611
Vertical Force F_y [μN]	Mean $\times 10^{-1}$	5.5486	5.5486	5.5486
	Std $\times 10^{-1}$	1.3489	1.3482	1.3488

Now we consider the effect of variation in the length of the movable finger L, while fixing the thickness to be $\overline{T} = 0.2$ μm. The length is again modeled as a random variable, and is written as $L(\theta) = \overline{L}(1 + v_L\xi)$, where ξ is a unit variance Gaussian random variable as before and v_L is the percentage variation in L. This variation is implemented by applying the random displacement $\mathbf{u}(\mathbf{x}, \theta) = [v_L(x - x_0)\xi, 0]^{\mathrm{T}}$ to the movable finger, where x_0 is the x-coordinate where the finger is attached to the movable center stage. We set $v_L = 0.02$, which represents a variation of 1.2 μm in the length. Similar results, as for the case of uncertain thickness, are shown in Fig. 12 and the corresponding mean and standard deviation values for capacitance and force are tabulated in Table 5.

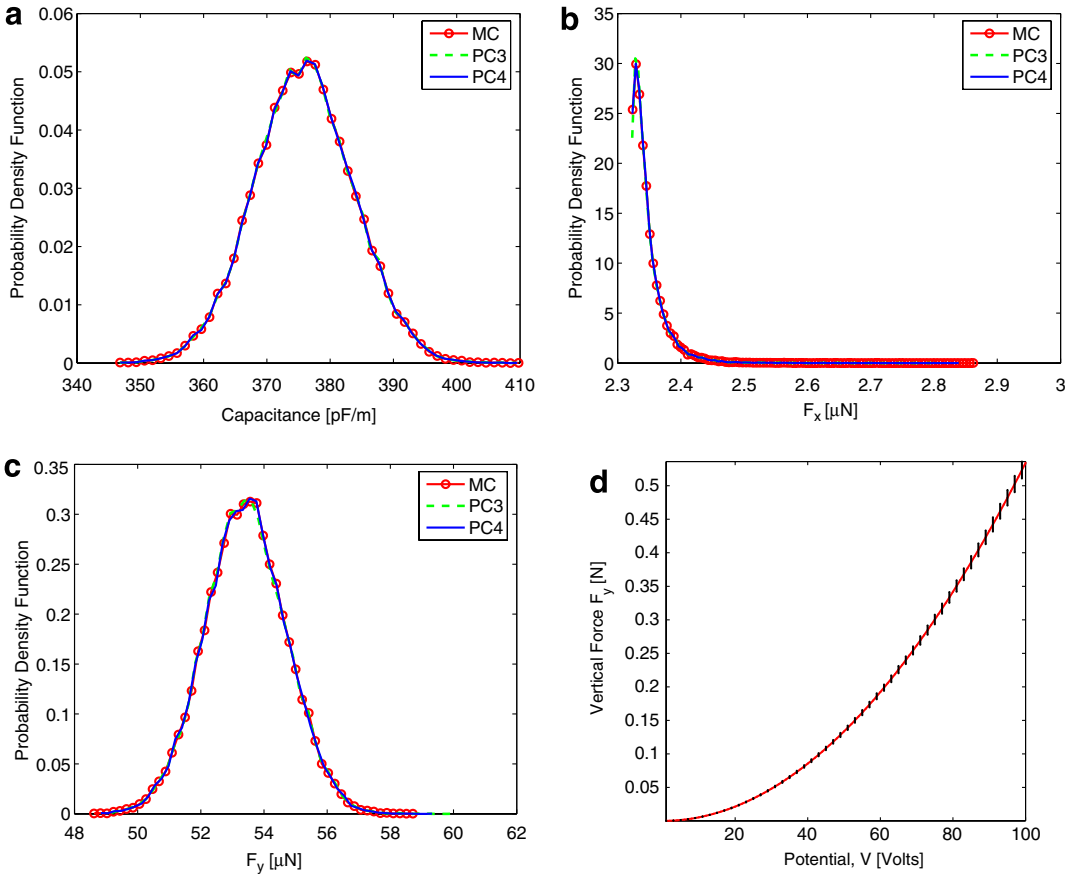

Fig. 12. Effect of variation in the length of the movable finger in the transverse comb drive on capacitance and net electrostatic force. (a) Probability density function of capacitance. (b) Probability density function of horizontal force F_x. (c) Probability density function of vertical force F_y. (d) Variation of mean and corresponding error bars of the vertical force with applied voltage V.

Table 5
Mean and standard deviation of capacitance and force for 2% variation in L

		MC	PC3	PC4
Capacitance [pF/m]	Mean $\times 10^{-2}$	3.7853	3.7853	3.7853
	Std $\times 10^{0}$	7.8315	7.8317	7.8316
Horizontal Force F_x [μN]	Mean $\times 10^{0}$	2.3472	2.3472	2.3472
	Std $\times 10^{2}$	2.6572	2.6461	2.6553
Vertical Force F_y [μN]	Mean $\times 10^{-1}$	5.3414	5.3413	5.3414
	Std $\times 10^{0}$	1.2812	1.2821	1.2813

5.4. Cantilever beam over ground plane

We now consider a cantilever beam of length $2a$ and thickness $T = 0.2$ μm, located at a gap g over a ground plane, Fig. 13. We study the effect of stochastic gap g, on the capacitance and the net vertical electrostatic force acting on the beam. The stochastic gap is modeled as a random field and we employ KL expansion to represent it in terms of random variables. We assume an exponential covariance kernel, given as

$$C(x_1, x_2) = v_g^2 \exp\left(\frac{-r}{b}\right), \tag{62}$$

where $r = |x_1 - x_2|$, is the distance between points x_1 and x_2, b and v_g are parameters which determine the number of terms in the KL expansion required for accurate representation of the field. The parameter b is known as the correlation length and it reflects the rate at which the correlation decays between two points. A higher value of b leads to rapid decay of the eigenvalues and hence lesser number of terms in the KL expansion. On the other hand, a lower value of b leads to more number of terms in the KL expansion. We note that for general choice of covariance kernel and domain, the eigenvalues and eigenfunctions need to be computed numerically. However, for this specific choice of exponential kernel and simple domain, analytical expressions exist for eigenvalues and eigenfunctions and are given in [14].

Using these eigenvalues and eigenfunctions the stochastic gap can be represented in terms of the random variables using KL expansion given in Eq. (1) as,

$$g(\mathbf{x},\theta) = \bar{g}(\mathbf{x}) + \sum_{i=1}^{\infty} \sqrt{\lambda_i}\xi_i(\theta) f_i(\mathbf{x}), \tag{63}$$

where $\bar{g} = 0.1$ μm is the average value of the gap. The eigenvalues for the exponential kernel for $a = 1$ μm, $b = 1$ μm and $v_g = 1$ are shown in Fig. 14.

Since the eigenvalues decay very rapidly, we choose only the first two eigenfunctions in the KL expansion to represent the stochastic gap. Thus, truncating Eq. (63) at $i = 2$ leads to,

$$g(\mathbf{x},\theta) = \bar{g} + \sqrt{\lambda_1} f_1(x)\xi_1 + \sqrt{\lambda_2} f_2(x)\xi_2, \tag{64}$$

where ξ_1 and ξ_2 are independent Gaussian random variables with unit variance. This random variation in the gap is implemented by providing a random translational displacement $\mathbf{u}(\mathbf{x},\theta) = \left[0, \sum_{i=1}^{2} \sqrt{\lambda_i} f_i(x)\xi_i\right]^{\mathrm{T}}$ to the beam. Various realizations of the random beam geometry together with the mean configuration are shown in Fig. 15.

The probability density functions for capacitance and net vertical electrostatic force for $V = 1$ V and $v_g = 0.1$, obtained using polynomial chaos expansion and Monte Carlo method are shown in Fig. 16. The polynomial chaos results are shown to be in agreement with the Monte Carlo results. The corresponding values of mean and standard deviation for capacitance and vertical force are shown in Table 6. The variation

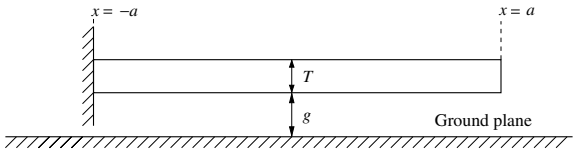

Fig. 13. Cantilever beam over a ground plane.

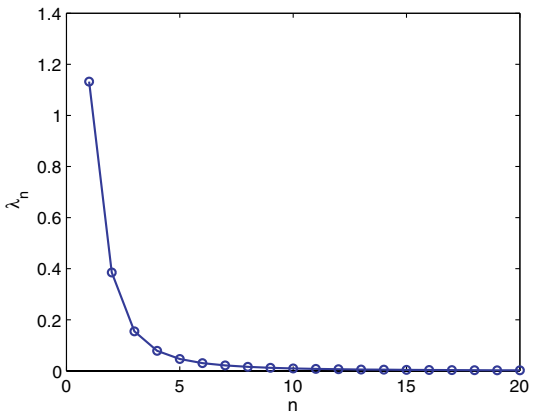

Fig. 14. Eigenvalues λ_n, $n = 1, \ldots, 20$ for the exponential covariance kernel, $a = b = 1$ μm, $v_g = 1$.

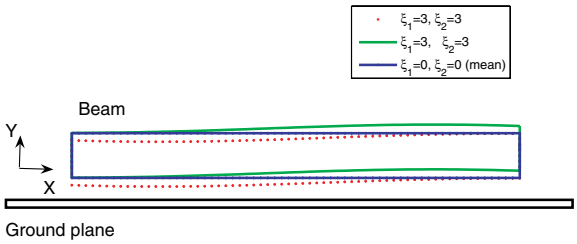

Fig. 15. Various realizations of the random configuration.

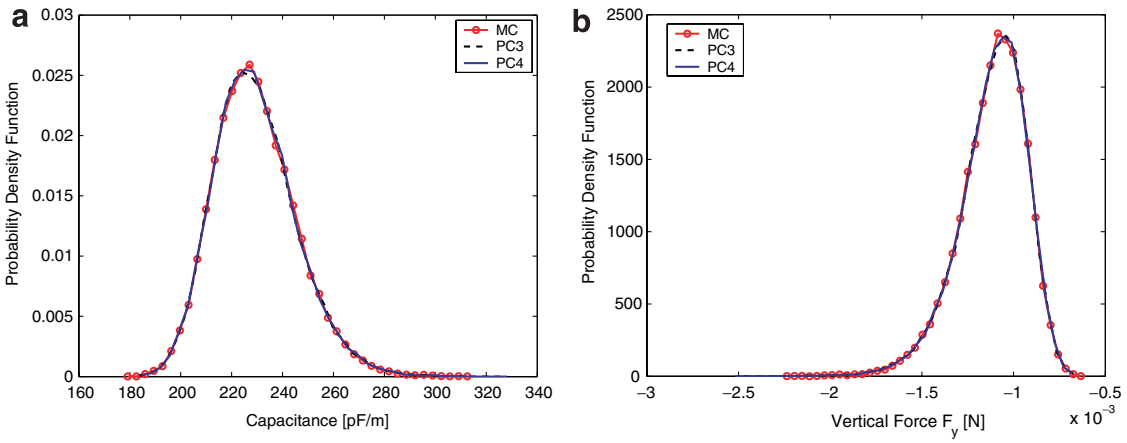

Fig. 16. Probability density functions for variation in the gap between the cantilever beam and the ground plane, [$v_g = 0.1$]. (a) Probability density function of capacitance. (b) Probability density function of net vertical force, $V = 1$ V.

Table 6
Mean and standard deviation of capacitance and force

		MC	PC3	PC4
Capacitance [pF/m]	Mean $\times 10^{-2}$	2.2937	2.2940	2.2940
	Std $\times 10^{-1}$	1.6154	1.6256	1.6258
Vertical force F_y [N]	Mean $\times 10^{3}$	−1.1167	−1.1171	−1.1171
	Std $\times 10^{4}$	1.8315	1.8474	1.8481

considered in the gap results in a variation of 7.0% and 16.5% around mean in the capacitance and vertical force, respectively.

6. Conclusions

This work presented a general framework to quantify uncertainty arising from geometrical variations in the electrostatic analysis. The variation in the geometry is modeled as a random field, which is expanded in terms of independent random variables using either polynomial chaos or Karhunen–Loève expansion. The uncertainty in the geometry is then used as a random displacement field in the Lagrangian boundary integral equation for electrostatics, to derive the stochastic Lagrangian boundary integral equation. The stochastic boundary integral equation is then discretized both in the random dimension and space using polynomial chaos with Galerkin projection and classical boundary element method, respectively.

We considered numerical examples arising from two different applications – first, we considered the modeling of interconnect circuits and studied the effect of geometrical variations on the capacitance. Second, we

studied the effect of variations in the dimensions and gap between the electrodes, on capacitance and net electrostatic force, during the analysis of MEMS. Using rigorous Monte Carlo simulations, it was shown that the proposed method accurately predicts the probability density functions and the statistics such as mean and standard deviation of these parameters. The polynomial chaos results were not only found to be in good agreement with the Monte Carlo results, but also converge to the MC results with the increase in the order of the chaos expansion. It has been shown in previous work [39,40], that the polynomial chaos is at least an order of magnitude faster than MC simulations for reasonable dimensionality. Thus, the proposed method is an effective tool to handle geometrical uncertainties arising in the electrostatic analysis in an accurate and efficient manner.

Acknowledgement

This work is supported by the National Science Foundation under grant number 0601479, DARPA, Semiconductor Research Corporation, and the Computational Science and Engineering program at UIUC.

Appendix A. Treatment of nonlinear terms

The spectral modes $\mathscr{G}_l$ and γ_l given in Eq. (37) can be computed in a straightforward manner by considering a Galerkin projection onto each basis Ψ_l,

$$\mathscr{G}_l(P,Q) = \frac{\langle \mathscr{G}(P,Q,\theta), \Psi_l \rangle}{\langle \Psi_l^2 \rangle}, \quad \gamma_l(Q) = \frac{\langle \gamma(Q,\theta), \Psi_l \rangle}{\langle \Psi_l^2 \rangle}, \tag{A.1}$$

where the integrals $\langle \mathscr{G}(P,Q,\theta), \Psi_l \rangle$ and $\langle \gamma(Q,\theta), \Psi_l \rangle$ are computed using numerical quadrature while $\langle \Psi_l^2 \rangle$ can be precomputed using the definition of the basis functions. For an appropriate quadrature rule, this direct integration procedure would always lead to accurate projections. However, this projection technique can be expensive as the number of random dimensions increases or when such projections need to be computed repeatedly. Such a situation may arise when the system is time dependent or is coupled with other physical fields such as mechanical or fluidic, which requires the computation of these projections at every time step or iteration step.

The spectral modes $\mathscr{G}_l$ and γ_l can also be computed in a reasonably efficient manner by using some arithmetic operations on random scalars as given in [41]. For a given source point P and field point Q, the nonlinear functions, $\mathscr{G}(P,Q,\theta)$ and $\gamma(Q,\theta)$ represent random scalars given as,

$$\mathscr{G}(P,Q,\theta) = -\frac{1}{2\pi\epsilon} \ln[d(\theta)]\gamma(Q,\theta) \tag{A.2}$$

$$\gamma(Q,\theta) = [\mathbf{T}(Q) \cdot \mathbf{C}(Q,\theta)\mathbf{T}(Q)]^{\frac{1}{2}} = [a(\theta)]^{\frac{1}{2}}, \tag{A.3}$$

where $d(\theta) = |P - Q + \mathbf{u}_P(\theta) - \mathbf{u}_Q(\theta)|$ represents the uncertain distance between the source and field points. Firstly, using the elementary operation for product of random scalars as given in [41], we express $a(\theta)$ and $d(\theta)$ in terms of the PC basis functions as

$$a(\theta) = \sum_{i=0}^{N} a_i \Psi_i, \quad d(\theta) = \sum_{i=0}^{N} d_i \Psi_i. \tag{A.4}$$

Further, we express $\ln[d(\theta)]$ and $[a(\theta)]^{\frac{1}{2}}$ in terms of the PC basis functions, using the approach for nonpolynomial functional evaluations for natural logarithm and square root respectively, as given in [41]. Finally, using these expansions in Eqs. (A.2) and (A.3) and the product operation, we obtain the spectral modes $\mathscr{G}_l$ and γ_l.

These operations make use of third-order tensor $C_{ijk} = \frac{\langle \Psi_i \Psi_j \Psi_k \rangle}{\langle \Psi_k^2 \rangle}, \{i,j,k \in [0,\ldots,N]^3\}$, which can be precomputed and stored to use throughout the computations. We must note that this approach works reasonably well for cases when the uncertainties in the field variables are moderate and the distribution functions of these variables are not too skewed. For the numerical examples considered in this work, it was verified that this approach leads to the same results as obtained using direct numerical quadrature.

References

[1] S.D. Senturia, N.R. Aluru, J. White, Simulating the behavior of MEMS devices: computational methods and needs, IEEE Comput. Sci. and Eng. 4 (1) (1997) 30–43.
[2] G. Li, N.R. Aluru, Efficient mixed-domain analysis of electrostatic MEMS, IEEE TransComput.-Aided Des. Integr. Circuits Systems 22 (9) (2003) 1228–1242.
[3] S.K. De, N.R. Aluru, Full-Lagrangian schemes for dynamic analysis of electrostatic MEMS, J. Microelectromechanical Systems 13 (5) (2004) 737–758.
[4] K. Nabors, J. White, FastCap: A multi-pole accelerated 3-D capacitance extraction program, IEEE Trans. Comput.-Aided Design 10 (1991) 1447–1459.
[5] F. Shi, P. Ramesh, S. Mukherjee, On the application of 2D potential theory to electrostatic simulation, Communications in Numer. Meth. Eng. 11 (1995) 691–701.
[6] J.D. Jackson, Classical Electrodynamics, Wiley, New York, 1999.
[7] G. Li, N.R. Aluru, A Lagrangian approach for electrostatic analysis of deformable conductors, J. Microelectromechanical Systems 11 (June) (2002) 245–254.
[8] S.K. De, N.R. Aluru, Coupling of hierarchical fluid models with electrostatic and mechanical models for the dynamic analysis of MEMS, J. Micromech Microeng. 16 (8) (2006) 1705–1719.
[9] S.M. Ross, Simulation, Academic Press, 2002.
[10] G.S. Fishman, Monte Carlo: Concepts, Algorithms, and Applications, Springer-Verlag, 1996.
[11] R.L. Iman, W.J. Conover, Small sample sensitivity analysis techniques for computer models, with an application to risk assessment, Commun. Stat. Theory Meth. A9 (1980) 1749–1842.
[12] R.L. Iman, W.J. Conover, Distribution-free approach to including rank correlation among input variables, Commun. Stat.-Simul. Comput. 11 (3) (1982) 311–384.
[13] M.D. McKay, R.J. Beckman, W.J. Conover, A comparison of three methods for selecting values of input variables in the analysis of output from a computer code, Technometrics 2 (1979) 239–245.
[14] R.G. Ghanem, P. Spanos, Stochastic Finite Elements: A Spectral Approach, Springer, 1991.
[15] N. Wiener, The homogeneous chaos, Am. J. Math. 60 (1938) 897–936.
[16] D. Xiu, G.E. Karniadakis, The Wiener–Askey polynomial chaos for stochastic differential equations, SIAM J. Scientif. Comput. 24 (2) (2002) 619–644.
[17] D. Xiu, G.E. Karniadakis, Modeling uncertainty in steady state diffusion problems via generalized polynomial chaos, Comput. Methods Appl. Mech. Eng. 191 (2002) 4927–4948.
[18] D. Xiu, G.E. Karniadakis, Modeling uncertainty in flow simulations via generalized polynomial chaos, J. Comput. Phys. 187 (2003) 137–167.
[19] D. Xiu, G.E. Karniadakis, A new stochastic approach to transient heat conduction modeling with uncertainty, Int. J. Heat Mass Transfer 46 (2003) 4681–4693.
[20] R.G. Ghanem, Probabilistic characterization of transport in heterogeneous media, Comput. Methods Appl. Mech. Eng. 158 (1998) 199–220.
[21] R.G. Ghanem, Higher order sensitivity of heat conduction problems to random data using the spectral stochastic finite element method, ASME J. Heat Transfer 121 (1999) 290–299.
[22] O.P. LeMâitre, O.M. Knio, H.N. Najm, R.G. Ghanem, A stochastic projection method for fluid flow I. basic formulation, J. Comput. Phys. 173 (2001) 481–511.
[23] O.P. LeMâitre, M.T. Reagan, H.N. Najm, R.G. Ghanem, O.M. Knio, A stochastic projection method for fluid flow. II. random process, J. Comput. Phys. 181 (2002) 9–44.
[24] R. Ghanem, W. Brzakala, Stochastic finite-element analysis of soil layers with random interface, J. Eng Mech. 122 (4) (1996) 361–369.
[25] P.L. Liu, D.A. Kiureghian, Finite element reliability of geometrically nonlinear uncertain structures, J. Eng. Mech. 117 (8) (1991) 1806–1825.
[26] S. Acharjee, N. Zabaras, Uncertainty propagation in finite deformations – A spectral stochastic Lagrangian approach, Comput. Methods Appl. Mech. Eng. 195 (2006) 2289–2312.
[27] G. Dasgupta, A.N. Papusha, E. Malsch, First order stochasticity in boundary geometry: a computer algebra BE development, Eng. Anal. Boundary Elem. 25 (2001) 741–751.
[28] R. Honda, Stochastic BEM with spectral approach in elastostatic and elastodynamic problems with geometrical uncertainty, Eng. Anal. Boundary Elem. 29 (2005) 415–427.
[29] S.M. Prigarin, Spectral Models of Random Fields in Monte Carlo Methods, VSP, Utrecht, 2001.
[30] M. Loève, Probability Theory, Springer, 1977.
[31] R.H. Cameron, W.T. Martin, The orthogonal development of nonlinear functionals in series of Fourier–Hermite functionals, Ann. Math. 48 (1947) 385–392.
[32] J.H. Kane, Boundary Element Analysis in Engineering Continuum Mechanics, Prentice-Hall, Englewood Cliffs, NJ, 1994.
[33] N.R. Aluru, J. White, An efficient numerical technique for electromechanical simulation of complicated microelectromechanical structures, Sensors and Actuators, Phys. A 58 (1997) 1–11.
[34] Z. Lin, Circuit sensitivity to interconnect variation, IEEE Transactions on Semiconductor Manufacturing 11 (4) (1998) 557–568.
[35] A. Brambilla, P. Maffezzoni, Statistical method for the analysis of interconnects delay in submicrometer layouts, IEEE Trans. on Comput.-Aided Des. of Integ. Circuits Systems 20 (8) (2001) 957–966.

[36] T. Sakurai, K. Tamaru, Simple formulas for two-and three-dimensional capacitances, IEEE Trans. Electr. Dev. 30 (2) (1983) 183–185.
[37] T. Imamura, M. Katayama, Y. Ikegawa, T. Ohwe, R. Koishi, T. Koshikawa, MEMS-based integrated head/actuator/slider for hard disk drives, IEEE/ASME Trans. Mech. 3 (3) (1998) 166–174.
[38] S. Reh, P. Lethbridge, D.F. Ostergaard, Quality based design and design for reliability of micro electro mechanical systems (MEMS) using probabilistic methods, in: 2000 International Conference on Modeling and Simulation of Microsystems, San Diego, CA, MSM 2000.
[39] M. Jardak, C.H. Su, G.E. Karniadakis, Spectral polynomial chaos solutions of the stochastic advection equation, J. Scientif. Comput. 17 (1–4) (2002) 319–338.
[40] O.P. LeMâitre, H.N. Najm, R.G. Ghanem, O.M. Knio, Multi-resolution analysis of Wiener-type uncertainty propagation schemes, J. Comput. Phys. 197 (2004) 502–531.
[41] B.J. Debusschere, H.N. Najm, P.P. Pebay, O.M. Knio, R.G. Ghanem, O.P. LeMâitre, Numerical challenges in the use of polynomial chaos representations for stochastic processes, SIAM J. Scientific Comput. 26 (2) (2004) 698–719.